4-2004

Computing the Liquid Crystal Director Field in Optical Phased Arrays

George F. Barrick

Philip J. Bos
Kent State University - Kent Campus, pbos@kent.edu

Charles E. Titus

Bruce K. Winker

Computing the liquid crystal director field in optical phased arrays

George F. Barrick
Case Western Reserve University
Department of Mathematics
10900 Euclid Avenue
Cleveland, Ohio 44106
and
Kent State University
The Liquid Crystal Institute
P.O. Box 5190
Kent, Ohio 44242
E-mail: gfb3@po.cwru.edu

Philip J. Bos, MEMBER SPIE
Charles E. Titus
Kent State University
The Liquid Crystal Institute
P.O. Box 5190
Kent, Ohio 44242

Bruce K. Winker
Rockwell Scientific Company
1049 Camino dos Rio
Thousand Oaks, California 91360

Abstract. Optical phased arrays using birefringent liquid crystals can efficiently steer a laser communication beam to a small angle. The algorithm presented derives a thickness for the liquid crystal cell and computes a sequence of voltages for the device electrodes that best deflects the beam.
[DOI: 10.1117/1.1666821]

Subject terms: optical phased array; beam steering; 2-D optical modeling; two frequency liquid crystal.

Paper 030297 received Jun. 20, 2003; revised manuscript received Aug. 28, 2003; accepted for publication Aug. 28, 2003.

1 Introduction

Liquid crystal optical phased arrays (OPAs) for the steering of laser communication beams are analogues of classical diffraction gratings. Devices based on the electrically controlled birefringence (ECB) cell can achieve efficient steering of the beam using components with sizes on the order of two to twenty times the wavelength of light inside the liquid crystal. These components are narrow transparent electrodes that shape the director profile along one dimension of a liquid crystal slab, and so influence the phase of a coherent self-apodizing beam passing through the device.[1] A two-frequency liquid crystal material exhibits dielectric anisotropies of opposite signs when exposed to different frequencies for the applied voltage. Such materials can favorably influence switching speed of the device by using a high frequency to drive the liquid crystal molecules to a state close to their zero voltage equilibrium conformation.

Overall steering efficiency, as measured by the far-field intensity directed into a desired angle by the diffracting elements of the OPA, is limited by the width of the flyback regions where the liquid crystal molecular conformation resets at the physical edges of each blaze within the device. Whenever the beam steering angle α for the device is small, shadowing caused by the resets is also small, and overall efficiency can be estimated using only the width of the flyback region relative to the total width of the device.[2] This work describes a procedure that lays out the minimum thickness (for fastest switching), and an optimum pattern of voltages to be applied to the device electrodes. Because the procedure gives an optimum voltage pattern, the larger outline of these experiments focuses on the effect of the number and size of the electrodes on the flyback region and consequent diffraction efficiency.

The reflective-mode optical phased array is a device that ideally imposes a linear profile on delay in the phase of a Gaussian beam across each blaze. The varying phase delay comes from a variation in the effective birefringence that results from changing degrees of alignment for the liquid crystal molecules along a single period of the array. The birefringence of the liquid crystal is controlled using transparent ITO electrodes along the bottom surface of the OPA that are powered at different voltages. Whenever the width b of the blazes of the array and the wavelength $\lambda = 1.55\ \mu$m of the light satisfy the grating condition

$$b \sin \alpha = m\lambda, \tag{1}$$

for the mth diffraction order corresponding to a normally incident wave and a steering angle of α radians, the waves emanating from discrete blazes are in phase with each other, and destructive interference of the waves is minimized. The steering angle α is on the order of 15 to 150 mrad (0.9 to 8.6 deg.). The use of a reflective material on the back face of the array means that the phase delay imposed by each segment of the device is doubled, and so the maximum single-pass delay is just $\lambda/2$.

2 Procedure for Device Optimization

Accurate design of the device phase profile is critical to the performance of optical phased arrays. The voltages applied to the electrodes must be carefully selected to ramp the phase delay linearly, in as much as this is possible. This can

 0091-3286/2004/$15.00

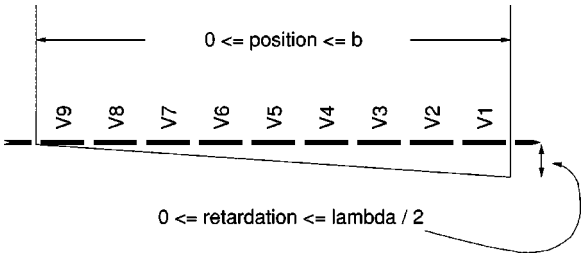

Fig. 1 Phase schematic of a reflective-mode OPA.

be accomplished by implementing a procedure that seeks to approximate an electro-optic curve for the liquid crystal that also incorporates the effects of elastic coupling between molecules, and the requirement for periodic sharp resets in the conformation.

Given a light source of wavelength λ μm and a specific steering angle α, the width b μm for periods of the array comes from the grating condition for an order $m=1$ diffraction grating described in Eq. (1). Within the width b μm of a blaze, the device should have N electrodes of equal widths having gaps between them large enough that distinct voltages can be applied to each electrode. For a liquid crystal material exhibiting optical birefringence Δn and dielectric response $\Delta\varepsilon$ to applied voltages, the goal of these computations is to use a cell thickness d μm as small as possible, and compute N optimal voltages that will produce a linear ramp of $\lambda/2$ μm in the phase of the lightwaves across the width b μm of a blaze.

The calculation of the voltages involves an electro-optic curve for the liquid crystal material that relates applied voltage to relative optical phase delay for impinging light. Given a material with particular Δn and $\Delta\varepsilon$, and impinging light of wavelength λ μm, the electro-optic curve is native to a device having a particular thickness d μm, and so it is necessary to establish cell thickness d before developing the appropriate electro-optic curve. Optical phase delay for a single pass through the device is half of a wave. However, the shortest optical path length possible for a material having birefringence Δn is not available, because an exceedingly high voltage would be needed to align the liquid crystal (LC) molecules in this conformation. Roughly, what the device requires is that the thickness d μm of the cell should give:

$$\Delta n \;\; d > \frac{1}{2}\lambda.$$

The first attempts at establishing d were along the lines of a ''guess and test'' procedure. A better way of estimating this quantity came up in the course of computational experiments.

Once a steering angle α is given, the blaze peridocity b μm and cell thickness d μm are mandated by calculations, and the results describe a ramp in the exiting phase of the light waves like that of Fig. 1. The number and spacing of ITO electrodes are the only parameters remaining free for the experimenter to arbitrarily select. For these parameters, the design of an optimal device consists of calculating voltages to be applied to the electrodes. The procedure for calculating the voltages can be summarized in terms of three computational modeling steps.

1. Develop an approximate electro-optic curve based on a 1-D LC model to predict a pattern of voltages for the OPA.
2. Model a 2-D LC director field associated with the voltages predicted by step 1, to observe phase delay as a function of position along the array. Voltages and mid-electrode phase delays from this curve are used to create a mathematical spline that provides more accurate estimates for the voltages. This process is iterated until an adequate phase profile is obtained.
3. Finite-difference time-domain optics for the 2-D LC director field (the computationally expensive kind) is used to evaluate the diffraction modes and efficiency of the proposed device.

To implement the first step of the procedure, the 1-D Frank-Oseen model is used to quickly compute the electro-optic response to applied voltages (and consequent birefringence) of the liquid crystal in parallel-aligned cells with specified pre-tilt. This was done using the GNU-LCM software[3] to solve for a liquid crystal director conformation $\hat{\mathbf{n}}(z)$ that depends on the polar tilt angle $\theta(z)$ for the director at every depth $z\in[0,d]$ via the relationship $\hat{\mathbf{n}}=(\sin\theta,0,\cos\theta)$. The goal for a given applied voltage V is to minimize the free energy

$$F=\frac{1}{2}(K_{11}\sin^2\theta+K_{33}\cos^2\theta)(\theta')^2 - \frac{1}{2}[\varepsilon_{\text{eff}}(\theta)]^{-1}\left\{\frac{V}{\int_0^d[\varepsilon_{\text{eff}}(\theta)]^{-1}}\right\}^2, \tag{2}$$

where $\varepsilon_{\text{eff}}(\theta)=\varepsilon_0(\varepsilon_\parallel\cos^2\theta+\varepsilon_\perp\sin^2\theta)$ by solving the associated Euler-Lagrange differential equation. This kind of model for electrically controlled birefringence devices (ECB cells) was run at voltages from 0.0 to 10.0 V in increments of 0.1 V for a one electrode device of the specified thickness d μm in configurations where polarizers at the top and bottom were either parallel or perpendicular. 1-D Berreman optics applied to the media gives the relative intensities $I_\parallel$ and $I_\perp$ for transmitted light. These depend on the phase ϕ of the emerging wave according to

$$I_\parallel=K\cos^2\left(\frac{1}{2}\phi\right),$$

$$I_\perp=K\sin^2\left(\frac{1}{2}\phi\right),$$

(where K is an arbitrary base intensity). The total delay $\Delta=(\phi/2\pi)\cdot\lambda$ μm can be recovered by computing

$$\Delta=\frac{\lambda}{\pi}\arccos\left[\left(\frac{I_\parallel}{I_\parallel+I_\perp}\right)^{1/2}\right] \tag{3}$$

at every voltage in the series.

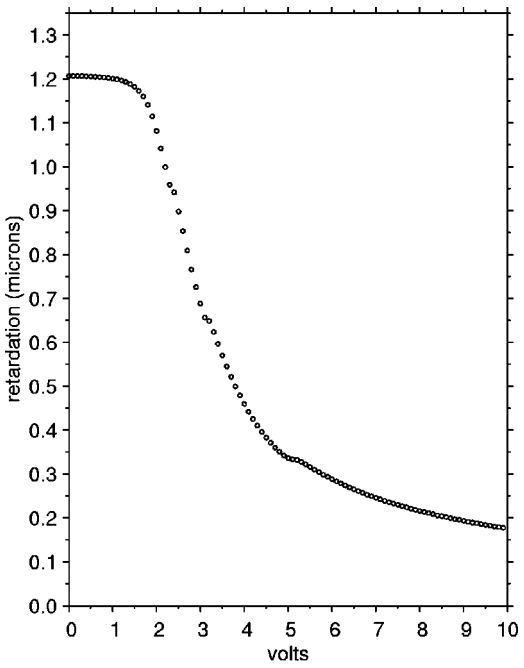

Fig. 2 Optical phase delay versus voltage for 6.0 μm cell.

The inverse cosine imposes several extrema on the graph of Δ versus voltage. Despite this, the delay decreases monotonically with decreasing polar tilt angle in the liquid crystal director, and so must always decrease with increasing voltage. An arithmetical unfolding of the curve for a $d=6.0$ μm cell gives the relationship depicted in Fig. 2 of the phase delay δ for a material having a dielectric response characterized by $\varepsilon_{\|}=6.32\varepsilon_0$ and $\varepsilon_{\perp}=3.10\varepsilon_0$ ($\varepsilon_0=8.854\times10^{-12}$ F$\cdot$m^{-1}), and optical birefringence $\Delta n=0.2214$.

To derive for an OPA cell a sequence of voltages to be applied to the electrodes of the device, we use an electro-optic curve like that of Fig. 2. The inverse of the function is used to map voltages associated with a sequence of phase delays positioned in proportion to the locations of the electrode centers along the width of the device. For a b μm wide device like that of Fig. 1 having N electrodes with centers spaced $u=b/N$ μm apart, the referenced phase delays are in sequence:

$$[u/(2b)]\cdot(\lambda/2),[3u/(2b)]\cdot(\lambda/2),\ldots,[(2N-1)u/(2b)]\cdot(\lambda/2) \tag{4}$$

above the minimum attainable retardation on the curve. Numerically, the voltages are computed from the phase delays by interpolating linearly between the closely spaced points of the curve.

With the voltages established, the second step of the method uses 2-D computational modeling of the liquid crystal conformation that results from the application of these voltages. This will supply a map of the directors between the plates of the device, as depicted for a $d=6.0$ μm cell in Fig. 3. The mathematical realization of this model is the minimization of the Frank-Oseen free energy

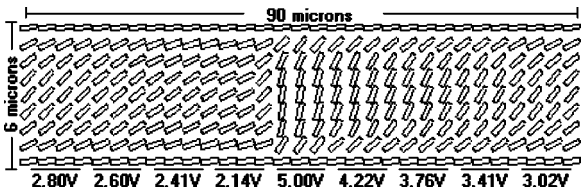

Fig. 3 Conformation (centered at the reset) for one blaze of a 6.0 μm cell.

$$F=\frac{1}{2}K_{11}(\nabla\cdot\hat{\mathbf{n}})^2+\frac{1}{2}K_{22}[\hat{\mathbf{n}}\cdot(\nabla\hat{\mathbf{n}})]^2+\frac{1}{2}K_{33}\|\hat{\mathbf{n}}(\nabla\hat{\mathbf{n}})\|^2-\frac{1}{2}\mathbf{D}\cdot\mathbf{E}, \tag{5}$$

where the director $\hat{\mathbf{n}}(x,z)$ varies in two dimensions using the associated Euler-Lagrange system of differential equations on a grid of nodes spaced about 0.25 μm apart. The electric free energy term $(1/2)\mathbf{D}\cdot\mathbf{E}$ in Eq. (5) is computed from the voltage gradient $\mathbf{E}=(\nabla V)^{\top}$ using

$$\mathbf{D}\cdot\mathbf{E}=\varepsilon_{\perp}\|\nabla V\|^2+\Delta\varepsilon[(\nabla V)\hat{\mathbf{n}}]^2.$$

The voltages $V(x,z)$ throughout the domain of the computation must satisfy the Coulomb-Gauss electric law, that $\nabla\cdot\mathbf{D}=0$ in a medium lacking free charges. Because the electric displacement arises from the dielectric tensor $\boldsymbol{\varepsilon}=\varepsilon_{\perp}\mathbf{I}+\Delta\varepsilon\hat{\mathbf{n}}\hat{\mathbf{n}}^{\top}$, the voltages must be computed anew at each step of the minimization. Stated in terms of V and $\hat{\mathbf{n}}$, the electric law requires that the sum

$$\varepsilon_{\perp}\nabla^2V+\Delta\varepsilon\{(\nabla V)(\nabla\hat{\mathbf{n}})+(\nabla\cdot\hat{\mathbf{n}})(\nabla V)+\hat{\mathbf{n}}^{\top}\mathbf{H}[V]\}\hat{\mathbf{n}}$$

be identically zero, where the gradient of V is interpreted to be a 1×3 row vector, and both the gradient of $\hat{\mathbf{n}}$ and the Hessian $\mathbf{H}[V]$ are 3×3 matrices.

The LC3D software[4] provides a convenient implementation of the 2-D Frank-Oseen model, where the anchoring of the liquid crystal molecules at the top and bottom plate and the periodic variation of the medium along horizontal scales of length b μm (the blaze width) provide boundary conditions for the problem. The important points to note are first, that the aligned liquid crystal does not give a stepped ramp, but rather due to the elastic interactions between the molecules, a relatively smooth variation in optical phase delay. Second, a profile of optical phase delay can be taken directly from the conformation map using a series of computationally inexpensive numeric integrals

$$\delta(x)=\int_0^d[n_{\mathrm{eff}}(x,z)-n_{\perp}(x,z)]dz, \tag{6}$$

(where $n_{\mathrm{eff}}=[\varepsilon_o\varepsilon_e/(\varepsilon_o+\Delta\varepsilon n_3^2)]^{1/2}$), along vertical slices of the device model. The profile can be adjusted and quickly derived again without recourse to full optical modeling of the device. A profile for a 6.0-μm device having nine electrodes can be seen in Fig. 4.

As demonstrated by Fig. 4, the voltages derived from the original electro-optic curve are not quite correct. However,

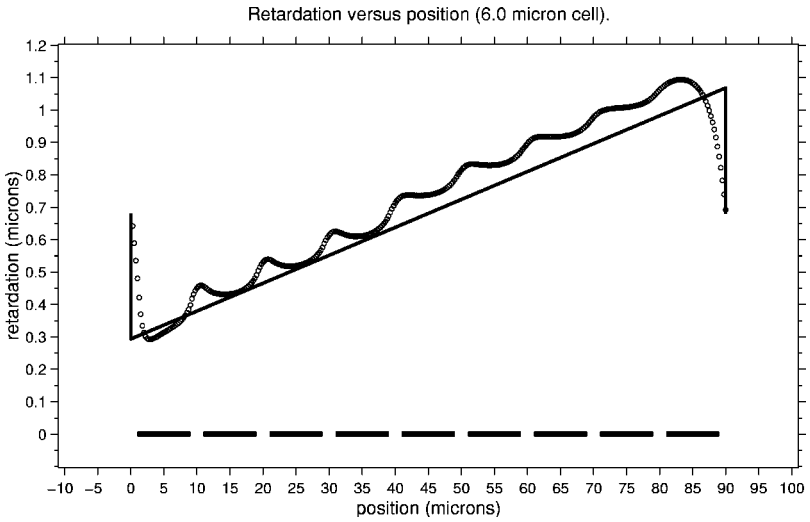

Fig. 4 Optical phase delay compared to an ideal profile.

the phase delay observed directly above the middle of each of the electrodes in this new graph ought to be more representative of the true response. The N voltages that were applied for this device, and the N optical phase delays that are associated with them at the midpoints of the electrodes in Fig. 4, can provide more accurate estimates for the voltages. A smooth ''not-a-knot'' spline function interpolating to these N voltage/phase delay observations, as depicted in Fig. 5, makes it possible to compute a new sequence of voltages from the original sequence in Eq. (4) of phase delays. The spline in Fig. 5 will enforce slightly higher voltages for the phase delay values near the high end of the required range, thus slightly decreasing the height of the curve on the right side of Fig. 4.

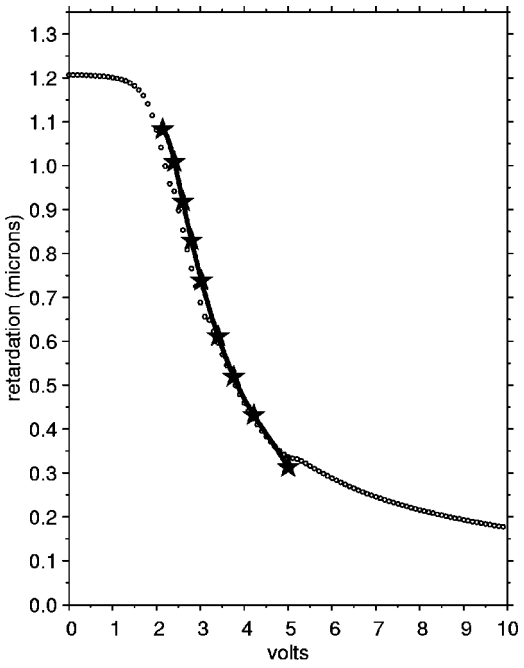

Fig. 5 Original optical phase delay with correcting spline.

The spline used in the process described here is a piecewise cubic polynomial that is second-order smooth at the knots where the definition of the cubic changes.[5] The knots are all of the interior data points, except for the second and the $(N-1)$st knots that are ''not knots,'' but rather are just data points to which the piecewise cubic must interpolate. Such a spline avoids the awkwardness of prespecified derivative or second derivative end conditions, but makes it necessary to use at least five distinct data points when creating the curve. The attractive feature of such a spline is that it provides a new electro-optic curve based on sparse data. Once the new voltages are computed using the inverse of the spline function on the phase delays in Eq. (4), another round of liquid crystal conformational modeling can be undertaken to give a new phase profile. This process may need to be repeated, but it soon yields voltages accurate enough to produce a phase profile like that of Fig. 6.

Phase delay profiles provided by the integrals in Eq. (6) do not indicate how well a series of several blazes acting as diffracting elements serve to steer a narrow Gaussian beam. To evaluate diffraction efficiency for OPAs, the third step of the modeling procedure, involving 2-D computational optics, is applied to the liquid crystal medium that results when using the optimum pattern of N voltages. The mathematics involved here is a finite-difference time-domain solution[6] of the Maxwell equations:

$$\nabla \times \mathbf{H} = \boldsymbol{\varepsilon} \frac{\partial \mathbf{E}}{\partial t}$$

$$\nabla \times \mathbf{E} = -\mu_0 \frac{\partial \mathbf{H}}{\partial t}, \tag{7}$$

where $\boldsymbol{\varepsilon}$ is the optical anisotropy of the liquid crystal medium. This method is computationally expensive, because the discrete grids on which it is implemented have node spacings on the order 1/20 of a wavelength of the impinging light (0.0775 μm). The resources for such models typically require a clustered computing environment. The conditions imposed along the boundary of the device avoid the

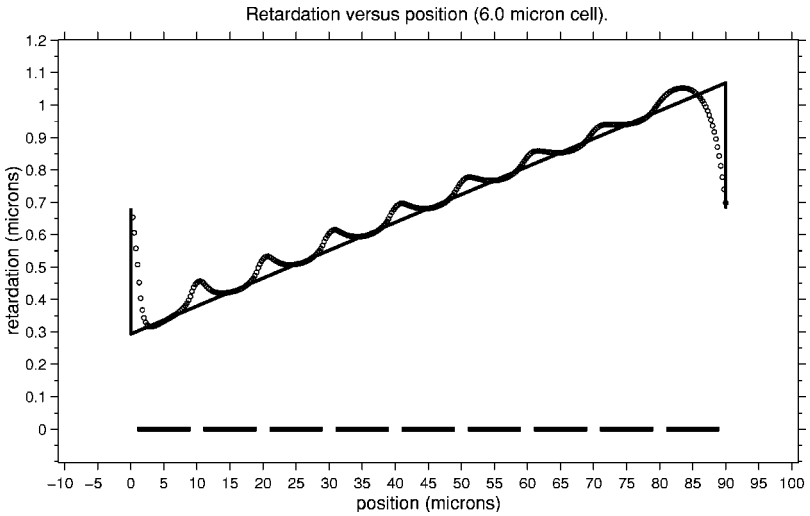

Fig. 6 Optical phase delay using revised voltages.

reflection of propagating waves back into the medium by using the perfectly matched layer technique.[7]

The electromagnetic fields produced on the exit surface of the device need to be transferred to the far field. A very accurate far-field diffraction pattern for a finite number of periods of the diffracting elements can be evaluated using the Helmholtz-Kirchoff integral as described by Titus et al.[8] The irradiance $I(\mathbf{r}')$ at a point location $\mathbf{r}'$, distant $R=\|\mathbf{r}'-\mathbf{r}\|m$ from the exit surface, is described by the integral

$$\frac{1}{4\pi}\int\int_S\left[I(\mathbf{r})\nabla\left[\frac{1}{R}\exp(ikR)\right]-\left[\frac{1}{R}\exp(ikR)\right]\times(\nabla I)(\mathbf{r})\right]\mathbf{n}dS, \tag{8}$$

where $k=\|\mathbf{k}\|$, S is the exit surface of the device, and $\mathbf{n}$ is the unit normal to the exit surface. The efficiency with which incident light energy is diffracted into the steering angle (in the case of the device of Fig. 6, $\alpha=17.2$ mrad) can be summarized via a plot similar to the one of Fig. 7, where the ratio of energy in the desired peak to total input energy is approximately 0.819. If all the light energy was deflected into a single diffraction order, the maximum of the plot would be 1.

3 The Modeled Devices

The phased arrays discussed here were designed to steer a $\lambda=1.55$ μm infrared laser with beam waist 250 μm into an angle of $\alpha=17.4$ mrad with the best possible efficiency. A second requirement was the capability to rapidly switch between deflecting and nondeflecting states of a device.

To achieve the rapid switching, the devices needed to be as thin as possible, while still exhibiting enough variation in birefringence that a ramp of $\lambda/2$ μm was possible. Assuming the use of infinite voltage, so as to vertically align all of the molecules in the device, and obtain the minimum value for phase delay, it might be expected that the thickness d μm could be chosen to have

$$\Delta n \quad d=\lambda/2.$$

The data sheet for the material MLC-2048 (from E. Merck Company) that was used in these experiments gives the figures $n_o=1.4978$ and $n_e=1.7192$ for optical anisotropy. These were valid for $\lambda=0.589$ μm. In the absence of further data, it was these same refractive indices that were used for the $\lambda=1.55$ μm infrared beam. So, with $\Delta n=0.2214$, and the assumption of infinite voltage, the value for $d=3.500$ μm. However, devices this thin cannot steer a laser beam.

The maximum voltage for the cells is 5.0 V, and this precludes the use of the low portion of electro-optic curves like that of Fig. 2. Since fields between electrodes can be very high near the bottom of these cells, it was also neces-

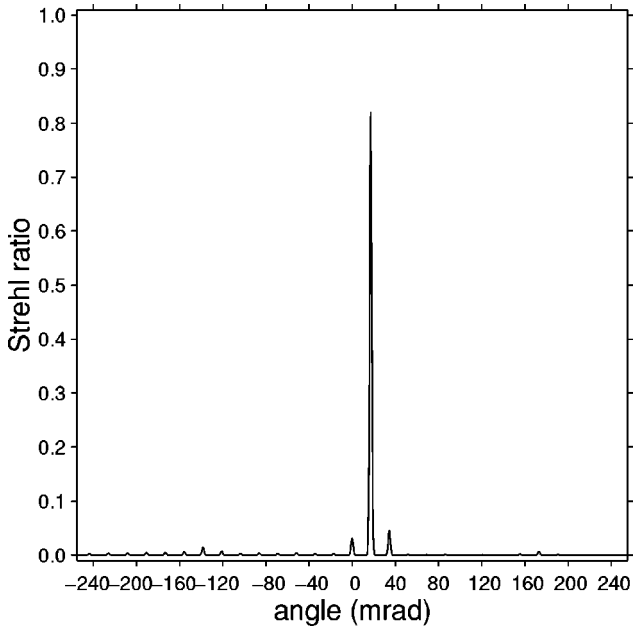

Fig. 7 Far-field diffraction pattern for device of Fig. 6.

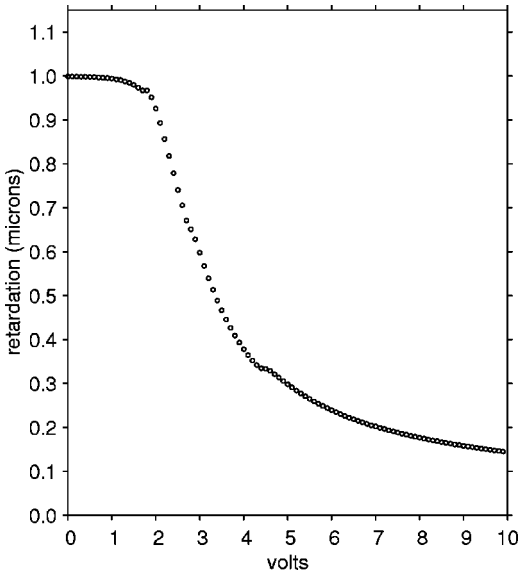

Fig. 8 Optical phase delay versus voltage for a 5.0 μm cell.

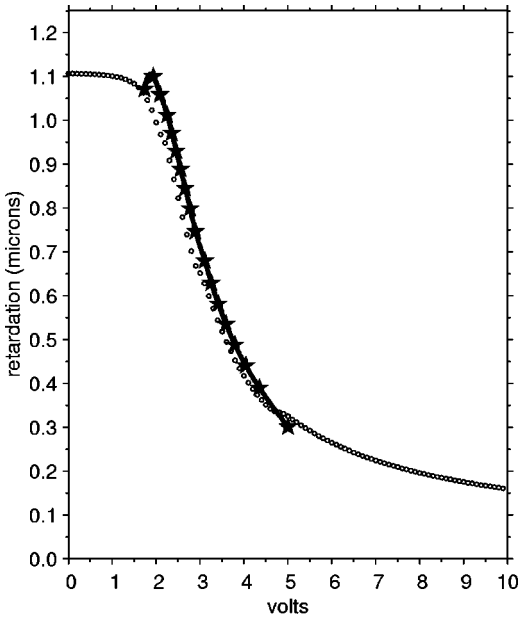

Fig. 9 Electro-optic curve and spline for 18 electrode $d=5.5$ μm cell.

sary to use a strong pretilt angle of 5 deg. for molecules next to the alignment layers at the top and bottom plates. This prevents all of the molecules in the cell from laying perfectly flat, and so precludes the use of the topmost portion of the electro-optic curve.

In practice, it has been necessary to adopt the rough rule that

$$\Delta n \quad d = 1.5(\lambda/2),$$

to have enough room on the resulting electro-optic curve for a ramp of $\lambda/2=0.755$ μm in the phase delay. For the cells modeled, this yields $d=5.251$ μm as the thinnest possible cell. Because cell spacers are typically available in increments of 0.5 μm, the thinnest cells here have $d=5.5$ μm. Some support for this rule comes from an electro-optic curve for a $d=5.0$ μm cell, where it is clear that a phase ramp of 0.755 μm is not attainable, because the top of the curve lies only 0.7 μm above the phase delay for 5.0 V (see Fig. 8).

Once the cell thickness $d=5.5$ μm had been selected, a first electro-optic curve was pursued for cells having 5 deg. pretilt, where the maximum permitted voltage is 5.0 V. Because the data sheet for MLC-2048 does not provide them, the elastic constants used were a trio of default values: $K_{11}=13.20\times10^{-12}N$, $K_{22}=6.50\times10^{-12}N$, and $K_{33}=18.30\times10^{-12}N$. This two-frequency liquid crystal material exhibits differing dielectric anisotropies (responses to applied voltage) depending on the frequency at which the voltage is applied. Molecules align perpendicular to an electric field at low frequencies, but align parallel with the field at frequencies beyond 10 kHz. A summary for the behavior of MLC-2048 appears in Table 1.

Table 1 Dielectric anisotropies for MLC-2048.

Frequency (kHz)	0.1	1.0	10.0	50.0	100.0
Anisotropy	3.28	3.22	0.72	−3.08	−3.40

Unfortunately, the absolute dielectric numbers for the two-frequency material were not listed, only the differences. The values $\varepsilon_\perp=3.10\varepsilon_0$, $\varepsilon_\parallel=6.32\varepsilon_0$ at 1.0 kHz, and $\varepsilon_\perp=6.18\varepsilon_0$, $\varepsilon_\parallel=3.10\varepsilon_0$ at 50.0 kHz were considered to be sufficiently representative of the material in question to be used for all of the computer modeling in these experiments.

An application for the high frequency anisotropy of MLC-2048 was suggested when observing the imperfect profile near the flyback regions between blazes of the optical phased arrays. Applying a voltage at high frequency to the electrode near the maximum of profiles like those of Figs. 4 and 6 might provide better control over the profile near the reset region. There is a good reason why this does not work.

The phase delay profiles for the cells that have been modeled all indicate that voltages less than 3.0 V always give phase delays greater than those that were expected from the first electro-optic curve. This is emphasized by the curve and the correction spline derived for a 5.5 μm cell with eighteen electrodes, which is depicted in Fig. 9. The correction for this elastic skewing of the curve is always to slightly increase the (low frequency) voltages on the offending electrodes, and so cause the molecules above them to tilt upward. Tilting of the molecules in this direction cannot be achieved using the high frequency voltage. A shift of the sequence in Eq. (4) of phase delays along the vertical axis to the top of the electro-optic curve does not alleviate the problem. Liquid crystal conformations using two frequencies in this way exhibit a strong lash, which shortens the total height of the electro-optic curve, making it difficult to compute an appropriate sequence of voltages.

To steer the beam to $\alpha=17.4$ mrad, the width b of the cell blazes needs to satisfy the condition in Eq. (1) for a first-order diffraction grating, and so $b=90.0$ μm in these

Table 2 Model diffraction efficiencies for a number of cells.

Thickness	*N*	Electrodes	Gap	Efficiency
5.5 μm	6	11 μm	4 μm	0.699
5.5 μm	6	13 μm	2 μm	0.778
6.0 μm	9	8 μm	2 μm	0.806
5.5 μm	9	8 μm	2 μm	0.819
5.5 μm	18	3 μm	2 μm	0.846

experiments. Only voltages in the low frequency (1.0 kHz) regime were used. Several $d=5.5$ μm cells and one 6.0 μm cell with varying numbers N of electrodes and different electrode widths were treated using the first two steps of the modeling procedure to obtain an optimal sequence of voltages for each. All of the devices were then subjected to 2-D optical modeling using a TM-polarized beam (beams with the TE-polarization pass undeflected), and evaluated with regard to diffraction efficiency. The (Strehl) ratio of light energy deflected into the primary $m=1$ diffraction order versus total input energy was derived from the far-field diffraction pattern exhibited by each of the cells. All of these diffraction efficiencies are presented in Table 2.

A useful property of the liquid crystal optical phased arrays is that they can be switched from steering the beam to allowing it to pass undeflected simply by powering down the electrodes. When exhibiting their high frequency response, molecules of MLC-2048 orient parallel to the electric field for voltages driven at 50 kHz. This provides an opportunity for OPA devices to be switched by applying the maximum voltage (5.0 V) at 50 kHz to all of the electrodes, causing all of the molecules in the device to lie flat, and then powering down so that they relax into their 5 deg. pretilt equilibrium conformation.

This high frequency switching is the primary reason for the interest in two frequency materials for displays and OPAs. An idea of the advantage in high frequency switching over simply allowing the material to relax down from

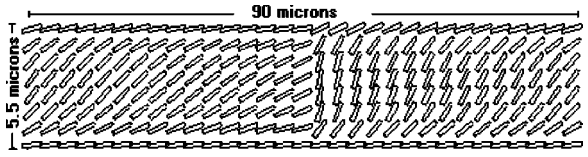

Fig. 11 Conformation for a $d=5.5$ μm ideal cell.

its steering conformation can be seen by computing the characteristic response times for the two modes. Using the formulas[9]:

$$\tau_{\text{relax}}=\frac{d^2\gamma_1}{\pi^2\kappa}, \quad \tau_{\text{rise}}=\frac{d^2\gamma_1}{V^2\varepsilon_0\Delta\varepsilon},$$

we can estimate both responses. For a $d=5.5$ μm cell (the thinnest practical one that was modeled), where $\gamma_1=0.111$ Pa·s and $\kappa=K_{11}=13.2\times10^{-12}N$, the time to relax down from the steering conformation is approximately 25.8 ms. To switch using 5.0 V at 50 kHz, we can compute τ_{rise} using $\varepsilon_0=8.85\times10^{-12}$ F·m^{-1} and $\Delta\varepsilon=3.08$ to get approximately 4.9 ms. This ignores the time it takes to go from the flattened conformation to the nearby relaxed state, but it does indicate that high-frequency switching is roughly five times faster than simply allowing the OPA to relax.

4 Results

All of the devices summarized in Table 2 implement sequences of voltages that provide a nearly linear phase ramp. Clearly, smaller electrodes provide finer control over the shape of the phase profile. A sense for how the diffraction efficiency depends on electrode placement can be gained by considering a theoretical best device.

For both $d=5.5$ μm and $d=6.0$ μm, the liquid crystal conformation files made it possible for us to construct an ''ideal'' device. These ideal devices were modeled by assembling columns from previously computed conformations to comprise devices with perfectly linear phase ramps. An example of such a profile for a $d=5.5$ μm device ap-

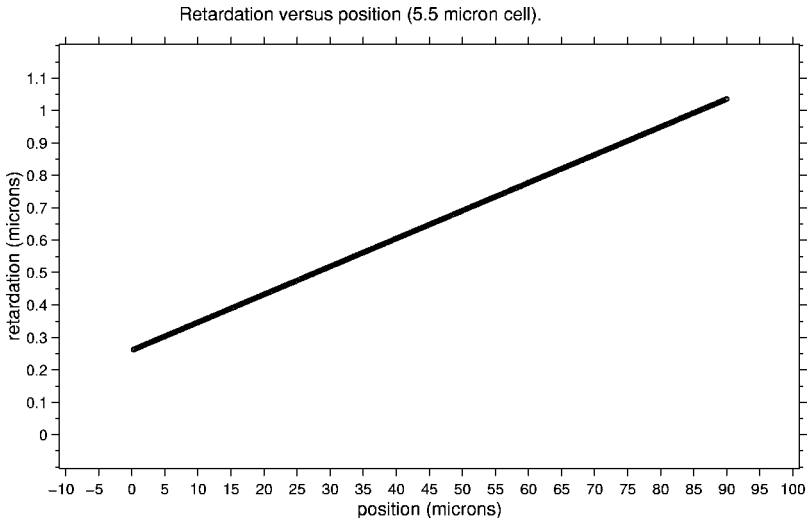

Fig. 10 Ideal phase delay profile for a $d=5.5$ μm cell.

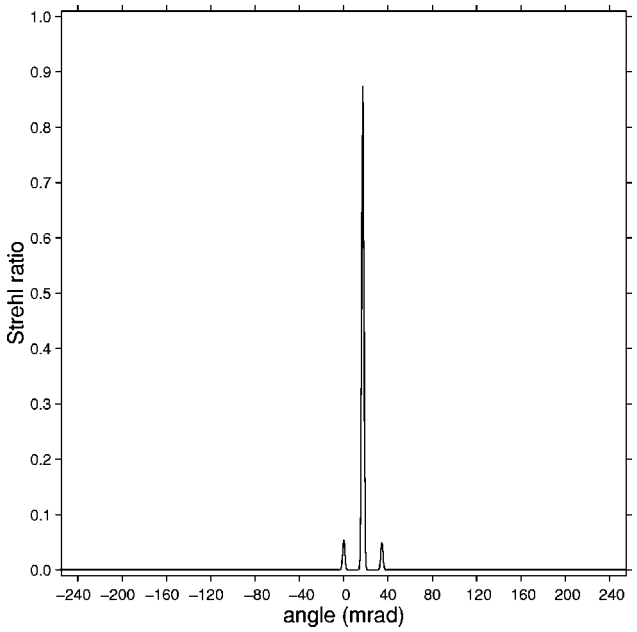

Fig. 12 Far-field diffraction pattern for an ideal $d=5.5$ μm device.

pears in Fig. 10. Its molecular conformation is depicted in Fig. 11. These devices are not derived from particular sequences of voltages. Adjacent columns of the material may come from different voltages. However, they can be subjected to optical modeling and evaluation of their diffraction efficiencies, as shown in Fig. 12.

These two, with diffraction efficiencies $\eta=0.870$ for the 6.0 μm cell and $\eta=0.874$ for the 5.5 μm cell, provide best attainable diffraction efficiencies against which the cells of Table 2 can be compared. Their diffraction efficiencies are not perfect, because:

1. blaze resets still have finite widths of about 0.25 μm (though this is negligible in the computational models),
2. partial reflections at the top of the device scatter light energy into undesirable diffraction orders.

Table 3 Normalized diffraction efficiencies for the cells.

Thickness	*N*	Electrodes	Gap	Efficiency
5.5 μm	6	11 μm	4 μm	0.800
5.5 μm	6	13 μm	2 μm	0.890
6.0 μm	9	8 μm	2 μm	0.926
5.5 μm	9	8 μm	2 μm	0.937
5.5 μm	18	3 μm	2 μm	0.968

The scattering can be estimated. Because molecules lie 5 deg. from flat along the top edge of the device, $n_{\text{eff}}=1.71713$ there. Light lost to backscattering as it arrives in the device must then be the proportion

$$r_p=\left(\frac{n_{\text{eff}}-n_{\text{air}}}{n_{\text{eff}}+n_{\text{air}}}\right)^2=0.064963$$

of total impinging light. This loss also occurs as light exits the device, and so we expect diffraction efficiencies of approximately 0.870 for these ideal beam steering devices.

In actual beam steering, there are usually some antireflection coatings layered on to the top plate of the device. Normalizing the data of Table 2 using the numbers for the two ideal devices gives Table 3. These diffraction numbers indicate what is achievable as far as efficiency for liquid crystal OPAs.

The profiles of phase delay depicted in Figs. 4, 6, and 13 seem to indicate that about one half the width of both the first and last electrodes do not contribute to the correct phase profile. This width at the blaze reset, the flyback region, is a feature necessitated by the interactions between the molecules. In the worst case, it seems to have a width equal to the average for the widths of the first and last electrodes. An estimate for diffraction efficiency that incorporates the width of the flyback region as a second multiplicative factor appears as Eq. (9).

Even when the electrodes are chosen to have widths on the order of or smaller than the cell thickness, the width of the flyback region becomes yet smaller. In Fig. 9, where the

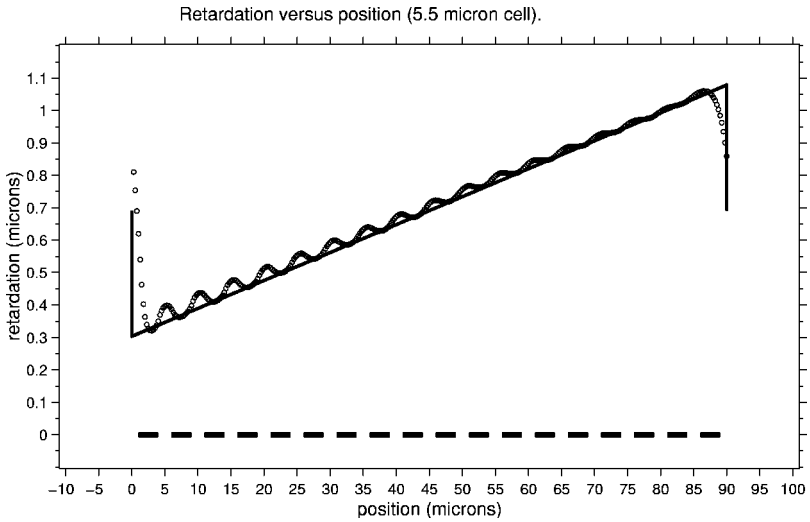

Fig. 13 Phase delay profile for an optimized 18 electrode 5.5 μm cell.

Table 4 Diffraction efficiencies for the cells, predicted using Eq. (10).

Thickness	N	Electrodes	Gap	η_{calc}
5.5 μm	6	11 μm	4 μm	0.892
5.5 μm	6	13 μm	2 μm	0.892
6.0 μm	9	8 μm	2 μm	0.927
5.5 μm	9	8 μm	2 μm	0.927
5.5 μm	18	3 μm	2 μm	0.963

spline indicates a lash in the electro-optic response measured near the last 3.0 μm electrode, the profile for this cell in Fig. 13 exhibits a flyback region that is less than 2.0 μm wide.

Estimates for diffraction efficiency based on both the flyback region and electrode number can be calculated using a version of the McManamon et al.[2] formula:

$$\eta=\left[\frac{\sin(\pi/N)}{\pi/N}\right]^2\left(1-\frac{f}{b}\right)^2, \tag{9}$$

where N is the number of electrodes, f is the width of the flyback region, and b is the total width of one blaze of the device. It was found that a better fit for the diffraction efficiencies from these experiments could be obtained by dropping the first factor in Eq. (9) to give the version:

$$\eta=\left(1-\frac{f}{b}\right)^2, \tag{10}$$

of the McManamon et al. formula. As a convenient way of summarizing the numerical results, the flyback region f can be taken to be approximately one third of the total width for a single electrode. The formula in Eq. (10) gives a convenient rule of thumb for the diffraction efficiencies of these devices whenever the gap between electrodes is smaller than the thickness of the cell. Examples of this calculation appear in Table 4, where it has been assumed that $f=(1/3)(b/N)$ in Eq. (10).

The overall efficiency of the optical phased array improves with increasing number of electrodes for the case of OPAs that steer a beam to low deflection angles. The small ripples that can be observed in Figs. 4, 6, and 13 are due to the gaps between electrodes. There are always slight drops of the base voltage in these gaps, and the liquid crystal conformation exhibits more rapid changes at these locations (but no disclinations) that give rise to the ripples in the phase profile. It is desirable to make these gaps as small as possible, though the available technology currently limits them to be greater than or equal to 2.0 μm. Because the vertical scale in the plots of Figs. 4, 6, and 13 is exaggerated by a factor of about 50, the ripples are actually small, typically smaller than one tenth of a wave, and do not appreciably effect the resulting diffraction efficiency.

5 Conclusions

Optical phased arrays based on two-frequency liquid crystal materials such as MLC-2048 can mimic the behavior of classical diffraction gratings. Specifically, the models described in this work indicate that arrays using a maximum of 5.0 V can steer coherent self-apodizing, $\lambda=1.55$ μm infrared laser communication beams to angles between 15 and 150 mrad with diffraction efficiencies nearing 95%. Though switching speeds were not modeled in these simulations, the negative dielectric anisotropy of the material at high frequencies is known from other studies to provide faster switching than that of cells where the liquid crystal simply relaxes into its 0.0 V conformation when the device is powered down. The three step modeling procedure described here makes it possible to design OPAs that achieve nearly optimal phase profiles. Computations of diffraction efficiency for these arrays agree with those postulated by McManamon et al., and exhibit the same trend with electrode number N.

Acknowledgments

The authors would like to thank Rockwell Scientific Company for support of this research.

References

1. P. F. McManamon, E. A. Watson, T. A. Dorschner, and L. Barnes, ''Applications look at the use of liquid crystal writable gratings for steering passive radiation,'' *Opt. Eng.* **32**(11), 2657–2664 (1993).
2. P. F. McManamon, T. A. Dorschner, D. L. Corkum, L. J. Friedman, D. S. Hobbs, M. Holz, et al., ''Optical phased array technology,'' *Proc. IEEE* **84**(2), 268–298 (1996).
3. S. Saeed and P. J. Bos, *Computer Modeling of Liquid Crystal Displays: GNU-LCM User Manual*, BosLab—The Liquid Crystal Institute, Kent State University, Kent OH 44242 (2001).
4. J. E. Anderson, P. E. Watson, and P. J. Bos, *LC3D: Liquid Crystal Display 3-D Director Simulator Software and Technology Guide*, Artech House, Norwood MA (2001).
5. J. Stoer, R. Bulirsch, R. Bartels, W. Gautschi, and C. Witzgall, *Introduction to Numerical Analysis*, 2nd ed., Springer-Verlag, New York (1997).
6. C. M. Titus, P. J. Bos, J. R. Kelly, and E. C. Gartland, Jr., ''Comparison of analytical calculations to finite-difference time-domain simulations of one-dimensional spatially varying anisotropic liquid crystal structures,'' *Jpn. J. Appl. Phys., Part 1* **38-1**(3A), 1488–1494 (1999).
7. J. P. Berenger, ''A perfectly matched layer for the absorption of electromagnetic waves,'' *J. Comput. Phys.* **114**, 185–200 (1994).
8. C. M. Titus, P. J. Bos, J. R. Kelly, E. C. Gartland, Jr., S. V. Shiaynovskii, and J. E. Anderson, ''Optical simulation of liquid crystal diffraction gratings,'' in *Technical Reports of the ALCOM Symposium: 2000 Digest, NSF ALCOM Science and Technology Center, The Liquid Crystal Institute*, **11**, 9–15 (2000).
9. L. M. Blinov, ''Electric field effects in liquid crystals,'' Chap. 5 in *Handbook of Liquid Crystal Research*, P. J. Collings and J. S. Patel, Eds., pp. 125–178, Oxford Univ. Press, New York (1997).

George F. Barrick is a visiting assistant professor at Case Western Reserve University. After completing his PhD in applied mathematics at Kent State University in 2000, he has collaborated with physicists at the Liquid Crystal Institute to investigate numerical methods suited to questions of computational physics for liquid crystal devices.

Philip J. Bos received his PhD degree in physics from Kent State University in 1978. After one year as a research fellow at the Liquid Crystal Institute at Kent State, he joined Tektronix Laboratories in the display research department. In 1994 he returned to the Liquid Crystal Institute, where he is currently an associate director and a professor of chemical physics. He currently has several projects in the area of applications of liquid crystals. He has more than 80 publications and 20 patents.

Biographies of other authors not available.